Heliyon 6 (2020) e04775

Contents lists available at ScienceDirect

Heliyon

journal homepage: www.cell.com/heliyon

Research article

Conformational & spectroscopic characterization, charge analysis and molecular docking profiles of chromone-3-carboxylic acid using a quantum hybrid computational method

K. Jayasheela [a], P.B. Nagabalasubramanian [b,*], S. Periandy [a]

[a] Department of Physics, Kanchi Mamunivar Centre for Postgraduate Studies, Puducherry, India
[b] Department of Physics, Arignar Anna Govt. Arts & Science College, Karaikal, Puducherry, India

ARTICLE INFO

Keywords:
Materials science
Materials chemistry
Theoretical chemistry
Chromone-3-carboxylic acid
DFT
Bacillus subtilis
Hirshfeld surface analysis
Charge analysis
Electronic properties

ABSTRACT

The Spectroscopic profile of Chromone-3-Carboxylic Acid (abbreviated as C3CA) was examined using FT-IR, FT-Raman, UV, ^{1}H and ^{13}C NMR techniques. The geometrical parameters and energies attained from DFT/B3LYP method with 6–311++G (d,p) basis sets calculations. The geometry of the molecule was fully optimized, vibrational spectra were calculated and assigned the fundamental vibrations on the basis of the total energy distribution (TED) of the vibrational modes, calculated with scaled quantum mechanics (SQM) method. The XRD data obtained from the computed geometric parameters shows that there is little deviation in the structure due to the substitution of the COOH group in the molecule. Using NBO study, the delocalization of the electron and the corresponding attraction between the orbitals shows that the lone pair transition has higher stabilization energy when compared with remaining atoms. The ^{1}H and ^{13}C NMR chemical shifts are calculated using GIAO method and the experimental chemical shifts were analysed with theoretical values which reflects better coincidence. The electronic properties, HOMO and LUMO energies, are performed with TD-DFT reproduces good with the experimental findings. Besides, frontier molecular orbitals (FMO), the high reactive nature of the molecule is identified with MEP and global reactivity descriptor analysis are performed. In addition, the molecular docking study was conducted, and results of the docking study identified the sugar phosphatase inhibitor activity of the target molecule (C3CA).

1. Introduction

Chromone-3-carboxylic acid is a heterocyclic compound (benzopyrone type), an isomer of coumarin with a substituted keto group of pyrone ring. Our human diet has some amount of Chromone and has a wide spectrum of biological activities. This molecule possess anti-oxide rutin activity [1], anticancer activity and used as interlenkin-5- inhibitors, monvamine oxidase inhibiors, neuroleptic agents [2]. Chromone is a natuarally occurring pharmo therapeutic compounds and its derivatives are used in the treatment of asthma. These compounds are used as antioxidant, anti-inflammatory, anti-allergic, anti-bacterial, anti-parasitic, anti-fungal, antimicrobial, anti-diabetic and anti-carcinogenic properties [3]. The bioactive nature of this molecule makes this candidate more effective in the medicinal chemistry. There are more studies in the derivatives of chromone [4, 5, 6, 7, 8, 9, 10, 11, 12, 13, 14].

By scrutinizing earlier studies, it is obvious that a study with hybrid quantum mechanical and molecular modeling approach on this title compound is not available. This study was to originate new perceptions into the structure and binding properties. To interpret the structural optimization, MEP, charge delocalization (NBO) and chemical shift (NMR), DFT Method was implemented. The derived optimized structure was utilized for docking the chromone 3-carboxylic acid to the biologically relevant metabolic protein.

2. Experimental details

The sample was collected from Sigma-Aldrich chemicals company, USA with 99% purity. The FT-Raman spectrum (400-4000cm^{-1}) of C3CA was recorded using Nd-YAG laser (1064 nm). By KBr pellet technique using IFS 66V spectrophotometer, IR spectrum (400-4000cm^{-1}) of the

* Corresponding author.
E-mail address: nagaphysics1975@gmail.com (P.B. Nagabalasubramanian).

https://doi.org/10.1016/j.heliyon.2020.e04775
Received 29 January 2020; Received in revised form 26 May 2020; Accepted 19 August 2020

compound was recorded. The compound with di-methyl sulphoxide (DMSO) solvent was prepared and NMR spectrum was taken between 20-200 ppm with the scanning interval of 20 ppm. With the aid of UV-1700 series instrument, UV-Visible spectrum was recorded between 200-400 nm, with the scanning interval of 0.2 nm.

3. Computational details

3.1. Quantum chemical calculations

The structure optimization, vibrational harmonic frequencies of the title compound are calculated using GAUSSIAN09 [15] package program using B3LYP/6311++G (d,p) basis set. The minimum PES has been obtained and the stability of the optimized geometries were confirmed by getting positive values to all the obtained wavenumbers. The relative contributions of the redundant internal coordinates to each normal vibrational mode of the molecule was analysed by calculating PED using VEDA4 program [16]. With the aid of GAUSSVIEW [17] program with symmetry considerations, vibrational frequency assignments were made with a high degree of accuracy. With the support of UV–Visible study using TD-DFT with same basis set, the major contributions in HOMO–LUMO energies, absorption wavelengths, oscillator strengths etc. based on the optimized structure in the solvent (DMSO) & in gas phase were calculated. Furthermore, MEP, the global reactivity descriptors were analysed. This study was also focused to envisage about Mullikan charges, Hirshfeld analysis, chemical shift (NMR) and charge delocalization of the title compound.

3.2. Molecular docking calculations

In order to attain further understandings on the molecule, molecular docking study was conducted. The ligand was prepared and stored in PDB file format. Then this ligand was imported into the AutoDock work space and the output was saved in PDBQT file format. For Protein preparation, AutoDock Protein preparation wizard was used. The sugar phosphatase inhibitor activity of the molecule was identified, and the suitable protein was selected for the same. The protein taken for the molecular dynamic simulation study is 4UAR (PDB ID) of Bacillus subtilis from Protein Data Bank. The polar hydrogens were added to satisfy the valency, lone pairs were merged to the selected protein, to mask the surface the water molecules were removed and the file was saved in a PDBQT file format. The receptor grids were generated using 90 Å x 90 Å x 90 Å grid size.

4. Result and discussion

4.1. Conformational analysis

The molecule has a carboxyl and pyrone substituent group attached to a benzene ring. By applying the PES technique, the structural confirmation was, in which the dihedral angle H_{20}–O_{18}–C_{15}–C_{12} is varied in 36 ways in steps of 10^0. The scanning graph is shown in Figure 1 which clearly depicts that two minimum energies were observed at 180° and 360° with -0.186 and -0.190 hartree respectively, which are structurally identical and acting as the most stable conformer of the compound. In addition, the maximum energy points at 260° is -0.172 hartree, which are considered as the least conformer.

4.2. Structural analysis

The crystal structure of the compound was reported previously [18] depicts that compound belong to monoclinic, $P2_1/n$ space with cell parameter a = 18.017 (8) Å, b = 5.549 (3) Å, c = 8.017 (5) Å, β = 92.49 (4) Å and Z = 4. The structure of the C3CA compound and experimentally

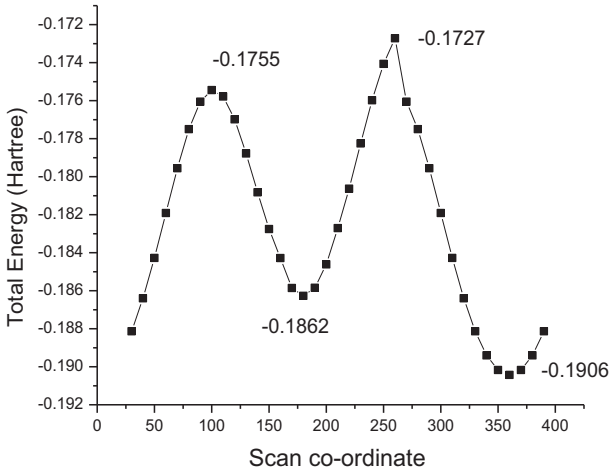

Figure 1. The potential energy curve of chromone-3-carboxylic acid.

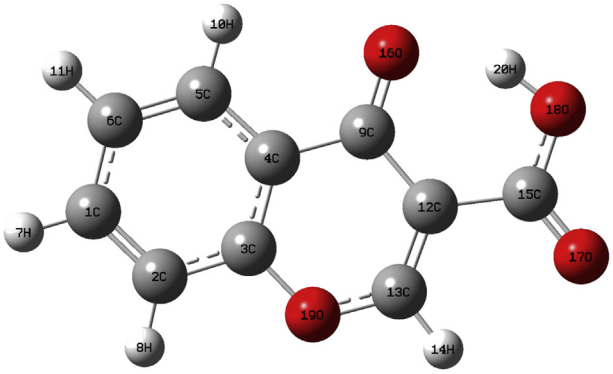

Figure 2. The structure of chromone-3-carboxylic acid.

determined XRD values are shown in Figure 2 & Table 1 respectively. In general, C–C–C angles of ipso atoms, which are known to be sensitive to the electronic properties of the substituent's [19]. The information about supplementary to the CIF pack is taken from Cambridge Crystallographic Database centre, No.CCDC. 1412580.

The C_3–C_4 bond is common for both benzene ring and substituted pyrone ring. The bond length calculated using computation method for C_3–C_4 is 1.39Å is almost equal to the experimental value. The theoretically observed other bond lengths C_1–C_2, C_2–C_3, C_4–C_5, C_5–C_6 and C_1–C_6 are compared with experimental one is well agreed with one another. In pyrone ring, due to single bond, C_4–C_9 and C_9–C_{12} bond lengths are 1.4Å while presence of two oxygen atoms O_{16} and O_{19} in this ring the bond C_{12} = C_{13} is 1.35Å which implies that it is purely double bond.

The bond lengths of C_9–O_{16} and C_{15}–O_{17} are1.23Å and 1.20Å respectively while that of C_{15}–O_{18}, it is 1.33Å. This difference in bond lengths of C–O group is mainly due to the bonding nature ie., the bonding nature between C_{15}–O_{18} (single bonded) and C_9–O_{16}, $C_{15}O_{17}$ (double bonded). Due to phase changes, the bond lengths obtained through theoretical method (gaseous phase) is higher than the experimental values (solid phase) The C–H bond lengths obtained from previous literature [20] was between 0.95 and 0.951 °A while of our theoretical values ranges between 1.0822 and 1.0837Å suggests that low scattering of hydrogen in X-ray diffraction makes larger deviation of C–H bond lengths which was not included in theoretical calculation. This overestimation is also verified in our calculation as represented in Table 1. Oxygen atoms in both ring has not influenced by the C–H bond lengths.

Table 1. Optimized Geometrical parameter for Chromone-3-Carboxylic acid Computed at B3LPY/6-311+G (d,p).

Bond Length (Å)		Methods B3LYP 6-311++G (d,p)	Exp.	Bond Angle (°)	Methods B3LYP 6-311++G (d,p)	Exp.
Benzene ring (C–C)				**Benzene ring (C–C–C)**		
C1–C2		1.3857	1.376	C1–C2–C3	118.54	118.7
C2–C3		1.3942	1.394	C2–C3–C4	121.90	121.8
C3–C4		1.3996	1.397	C3–C4–C5	118.40	118.7
C4–C5		1.4052	1.404	C4–C5–C6	120.32	119.7
C5–C6		1.3831	1.384	C1–C6–C5	120.07	120.2
C1–C6		1.4039	1.402	C2–C1–C6	120.74	120.9
Pyrone ring (C–C)				**Pyrone ring (C–C–C)**		
C4–C9		1.4704	1.464	C3–C4–C9	119.88	119.6
C9–C12		1.4601	1.445	C5–C4–C9	121.70	121.7
C12–C13		1.3555	1.348	C4–C9–C12	114.87	115.2
Benzene ring (C–H)				C9–C12–C13	119.77	120.6
C1–H7		1.0837	0.951	C9–C12–C15	122.97	115.7
C2–H8		1.0827	0.950	**Benzene ring (C–C–H)**		
C5–H10		1.0832	0.950	C2–C1–H7	119.39	119.6
C6–H11		1.0832	0.950	C6–C1–H7	119.86	119.5
Pyrone ring (C–H)				C1–C2–H8	122.03	122.7
C13–H14		1.0822	0.950	C3–C2–H8	119.42	120.7
Pyrone ring (C–O)				C6–C5–H10	121.73	120.2
C3–O19		1.3756	1.379	C4–C5–H10	117.94	120.1
C13–O19		1.3358	1.344	C1–C6–H11	119.81	119.9
C9–O16		1.2374	1.248	C5–C6–H11	120.10	119.8
C15–O17		1.2070	1.213	**Pyrone ring (C–C–H)**		
C15–O18		1.3338	1.323	C12–C13–H14	122.37	121.8
Out of rings				**Pyrone ring (C–C–O)**		
C12–C15	1.5074		1.497	C4–C9–O16	122.30	121.9
O18–H20	0.9893		0.840	C12–C9–O16	122.81	122.9
				C12–C13–O19	124.88	124.3
				C2–C3–O19	116.75	116.6
				C4–C3–O19	121.34	121.6
				Ring (C–O–C)		
				C3–O19–C13	119.23	118.8
				Ring (C–O–H)		
				C13–O19–H14	112.73	117.7
				Out of rings		
				C12–C15–O17	121.99	132.2
				C12–C15–O18	115.40	110.5
				O17–C15–O18	122.60	121.1
				C15–O18–H20	109.26	109.4

Taken from ref. [30].

The C–O bond length values of C_3–O_{19} and C_{13}–O_{19} present in the pyrone ring are 1.37Åand 1.33Årespectively shows higher values than the other C–O bonds. The bond length between the hydroxyl group (O_{18}–H_{20}) is 0.9893 Å is the lowest value than all other bonds present in the compound. The C_{12}–C_{15}, i.e. C_{pyrone}–$C_{carboxylic\ acid}$, bond length calculated by theoretical calculation is 1.5075 Å which is very close to the experimental value (1.497 Å).

The molecule with sp^2 hybridization. suggests that the bond angles observed are expected to be in the range of 120^0 but here, the bond angles vary from 117^0 to 122^0 may be due to substitution effects. Also, due to electronic conjugation among the bonds and presence of oxygen atom, there are small variations in the bond angles from the expected value of 120^o Additionally, it is observed that the electronic conjugation is lesser in benzene ring while higher in pyrone ring.

4.3. Mullikan and natural atomic charge analysis

Population analysis is constructed on the LCAO and the wave function of the molecule uses the density matrix (P) and the overlap matrix (S) to build the population matrix. MPA explains about the atomic charges, dipole moment, electronic structure and biological activity of the molecule. As the biological activity increases, the charge on the atom also increases [21]. The charges on the C3CA was computed by MPA & NAC and compared in the Table 2.

MPA predicts that the charge on C_1 atom shows the substitution of carboxylic group which will redistribute electronic charge over the chromone ring system. In benzene ring, charges on C_4, C_7, C_{11}, C_{12} and H_8, H_{10}, H_{11} are positive while others are negative and in case of pyrone ring, the charges on H_{14}, C_{15}, H_{20} are positive, C_4 is highly positive, C_3 is

Table 2. Mullikan Charges and NAC of Chromone-3-Carboxlic acid.

Atoms	Mullikan Atomic Charge	Natural atomic Charge
	B3LYP/6-311+G (d,p)	
C_1	-0.22779	-0.16963
C_2	-0.16411	-0.22119
C_3	-1.56454	0.34275
C_4	1.95887	-0.17557
C_5	-0.11718	-0.15014
C_6	-0.16941	-0.1971
H_7	0.14486	0.21465
H_8	0.14278	0.22297
C_9	-0.37049	0.50276
H_{10}	0.16304	0.23653
H_{11}	0.14171	0.21373
C_{12}	0.76583	-0.26374
C_{13}	-0.40561	0.24131
H_{14}	0.19524	0.19425
C_{15}	0.12549	0.77377
O_{16}	-0.32889	-0.52357
O_{17}	-0.31274	-0.50512
O_{18}	-0.21584	-0.69127
O_{19}	-0.04791	-0.51071
H_{20}	0.28664	0.46532

highly negative, C_{12} is very low positive and C_{13} is very low negative in the molecule.

NAC shows that charges on C_3, C_9, C_{13}, C_{15} are positive while others are negative. All H_7, H_8, H_{10}, H_{11}, H_{14}, H_{20} has positive charges which are attached with carbon in the carboxylic group whereas all the oxygen have negative charges.

4.4. NMR analysis

In this study, ^{1}H and ^{13}C chemical shifts of the title molecule in gas and DMSO solvent with DFT theory and the experimental NMR in DMSO Solvent are gathered in Table 3. The experimental ^{1}H and^{13}C NMR spectra of the C3CA are given in Figures 3 and 4 respectively. Primarily, the full geometry optimization of the molecule was performed at the gradient corrected DFT using the hybrid B3LYP method and GIAO [22, 23, 24]. ^{1}H and ^{13}C chemical shift calculations of the compound was made by the same method using 6–311++G (d,p) basis set in gas and DMSO solvent.

Electron-withdrawing atom or group can decrease the shielding and move the resonance of attached proton towards the higher frequency, whereas electron-donating atom or group increases the shielding and moves the resonance towards the lower frequency [21]. The chemical shifts of aromatic protons of organic molecules are usually observed in the range of 7.00–9.00 ppm.

The signals of 4 aromatic protons (1H) were calculated theoretically as 8.2–8.4, 7.7–8, 8.8–8.9 and 7.7–8.8 ppm for gas and DMSO solvent, respectively. These theoretically obtained values were verified with the reported experimental values in DMSO solvent at 8.1,7.9,7.7 and 7.6 ppm respectively in Table 3.

From the computed and experimental chemical shift values, H_7, H_8, H_{10} & H_{11} attached to the carbon atoms of the benzene ring has smaller values than the pyrone ring proton (H_{14}) and carboxyl proton (H_{20}) signals are due to the electronic charge density around the ring.

In experimental ^{13}C NMR spectrum (DMSO), the value of δ (chemical shift) of carbon atoms is absorbed between 118-176 ppm. The molecule has ten carbons however these carbons are differentiated in three groups (attached with benzene, pyrone, carboxyl) which is consistent with the structure and molecular symmetry. The chemical shift δ of the carbons present in the benzene ring (C_1 to C_6) are 135, 118, 155, 123, 125 & 126 ppm respectively; in the pyrone ring (C_9, C_{12} and C_{13}) are 176,114,163 ppm while the carbon present in carboxyl group (C_{15}) has δ of 163 ppm. The chemical shift (theoretical) in gas phase and DMSO solvent are presented in Table 3. The value of δ for C_9 & C_{13} attached in the pyrone ring is larger and the value of δ for C_{12} is very less than others due to the substituent effect of the carboxyl group. The absorption peak value of C_9 and C_{15} are larger (176 & 163 ppm) due to carbon-oxygen double bond.

4.5. Vibrational analysis

The C3CA molecule consists of 20 atoms with 54 normal modes of vibrations and considered under C_s point group symmetry. The computed and recorded FTIR spectra are as shown in Figures 5 and 6. The FT-IR and FT-Raman experimental frequencies, unscaled and scaled vibrational frequencies and PED of C3CA are calculated using B3LYP method with 6–311 G (d,p) basis set and tabulated in Table 4. The fundamental frequencies are assigned using PED values. The difference of values in theoretical and experimental frequencies are due to the over estimation of force constants in the quantum calculations, combination of electron correlations effects, and basis set deficiencies. To attain the closer difference between experimental and theoretical one, the theoretical values are scaled with the scaling factor of 0.99.

4.5.1. O–H vibrations

The OH group stretching vibrations in the carboxylic acid occurs between 3300 -2500 cm^{-1} and O–H bending from 1440-1395 and 950-910 cm^{-1}. Also, the chromone ring is attached with a single O–H group makes the stretching vibration of OH around 3300 cm^{-1} [25]. In this study, the O–H stretching vibration is assigned at 3183cm^{-1},in-plane and out-of-plane bending vibrations at 1438 cm^{-1} and 849 cm^{-1} (FT-Raman) respectively shows that the decrease in the wavenumbers is due to the substituent effect of chromone ring.

4.5.2. C–H vibrations

The hetero aromatic structure shows the presence of C–H stretching vibrations in the region 3000–3100 cm^{-1}. The strong vibration at 3089 cm^{-1} (FTIR), weak vibration at 3073 cm^{-1} (FT-R), medium vibration at 3071, 3062 and 3052 cm^{-1} in FTIR are due to C–H stretching modes. In this work, C–H in-plane bending vibrations are assigned at 1095 (FT-R), 1089, 1017 (FTIR) and 953 cm^{-1} (FTIR) and out of plane bending vibrations are assigned at 794 (FT-R), 751 (FTIR), 728 (FT-R), 697 (FTIR), 689 cm^{-1} (FT-R).

Table 3. Calculated ^{1}H and^{13} C NMR Chemical shifts (ppm) of Chromone-3-Carboxylic acid at B3LYP/6311++G (d,p) basis set.

Atom	Gas (ppm)	DMSO (ppm)	Experimental DMSO
C_1	135	137	135
C_2	118	120	118
C_3	156	157	155
C_4	124	123	123
C_5	129	127	125
C_6	127	128	126
C_9	177	178	176
C_{12}	114	113	114
C_{13}	163	166	163
C_{17}	161	164	163
H_7	8.4	8.2	8.1
H_8	7.7	8.0	7.9
H_{10}	8.9	8.8	7.7
H_{11}	8.8	7.7	7.6
H_{14}	9.0	9.0	9.1
H_{20}	13	13	13

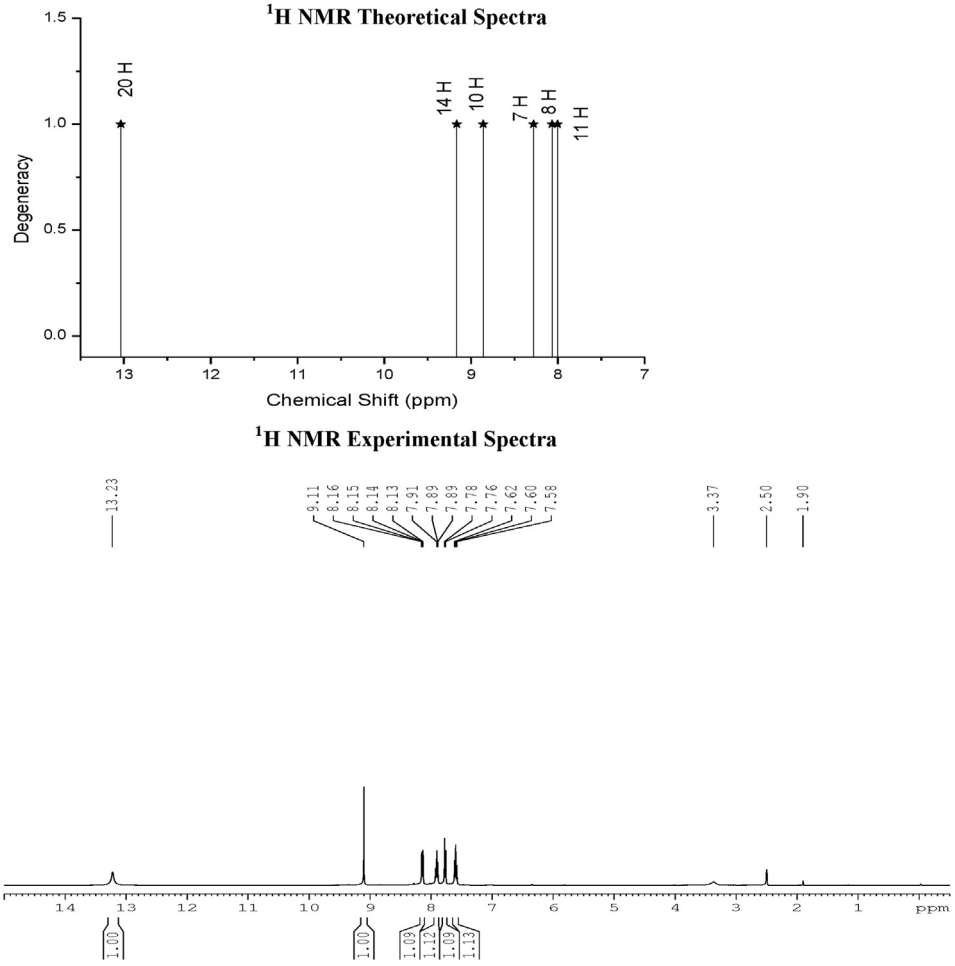

Figure 3. ^{1}H NMR Theoretical and Experimental Spectra of Chromone-3-carboxylic acid.

4.5.3. Ring vibrations

The C=C stretching vibrations are assigned in the range 1650-1500 cm^{-1} and C–C stretching vibrations are assigned in the range 1500-1400 cm^{-1} in previous literature [26]. In this work, the C=C stretching vibrations are assigned at 1580 cm^{-1} (FT-R), 1562 cm^{-1} (FTIR), 1544 cm^{-1} (FT-R) and 1432 cm^{-1} (FTIR). Similarly, C–C stretching vibrations in the regions are assigned at 1263, 1251, 1183, 1110 cm^{-1} in FT-IR and 1260, 1248, 1225, 1117, 1130 cm^{-1} in Raman spectra respectively. The theoretical C–C stretching wavenumbers are observed at 1276, 1234, 1220, 1170, 1144, 1123, cm^{-1}. The torsion and CCC bending modes are mixed with other modes.

4.5.4. CO vibrations

As per the previous literatures, the C=O stretch of carboxylic acids appeared between 1740-1660 cm-1 which is similar as C=O stretch in ketones. Also, the C=O asymmetric and symmetric stretching should be expected at 1832 cm^{-1} and 1761 cm^{-1} respectively. In this present work, the C=O asymmetric stretching at 1737 cm^{-1} (FTIR) with strong intensity and 1734 cm^{-1}(FT-R) with weak intensity. Similarly, the strong intensity peak at 1615 cm^{-1} (FTIR) and very strong peak at 1608 cm^{-1} (FT-R) is assigned to the symmetric C=O stretching vibration. The variation in expected frequencies shows the effect of substituents. Theoretically, the C=O stretching vibrations are observed at 1667 and 1691 cm^{-1} respectively. The C–O stretching vibrations are assigned to the weak FT-Raman peaks at 1402, 1360 and 1320 cm^{-1}. The in-plane bending vibrations of C=O are assigned at 926 cm^{-1} (FT-R) and 898 cm^{-1} (FTIR) frequencies. The C=O out of plane bending vibrations are assigned to the strong band at 620 (FTIR), 624 cm^{-1} (FT-Raman) and medium intensity peak at 548 cm^{-1} (FTIR).

4.6. Hirshfeld and finger print analysis

The hirshfeld surface on the title molecule is analysed with crystal explorer 3.1 software [27] to draw the 3D image of hirshfeld surface and is used to study the intermolecular interactions in detail. The two factors, 'd_e', the distance between any surface point nearest to interior atom, and 'd_i', the distance between the surface point nearest to the exterior atom are noted with vanderwaals radii of the atom. The mapping of hirshfeld shape index (-1.0000 to 1.0000), curvedness (-4.000 to 0.4000), surface over d_{norm} (-1.2738 to 1.1038), d_i (0.6990–2.4462), d_e (0.2903–2.2232) are shown in Figure 7. The observed fingerprints are shown in Figure 8, plotted using d $_{norm}$ descriptor which indicates the contributions of inter contacts to the Hirshfeld surfaces, C–H…H–C (42.1%), O–C…C–O (12.1%), C–C…C–C (7.2%), H–O...O–H (36.5%), and O–O...O–O (2.2%). The inter contacts in the hydrogen bonds are represented by the red spots over the surface.

From the shape index diagram, the red triangles in the concave region (above the plane of the molecule) indicating that the atoms of the π-stacked molecule above them, and the blue triangles represent by

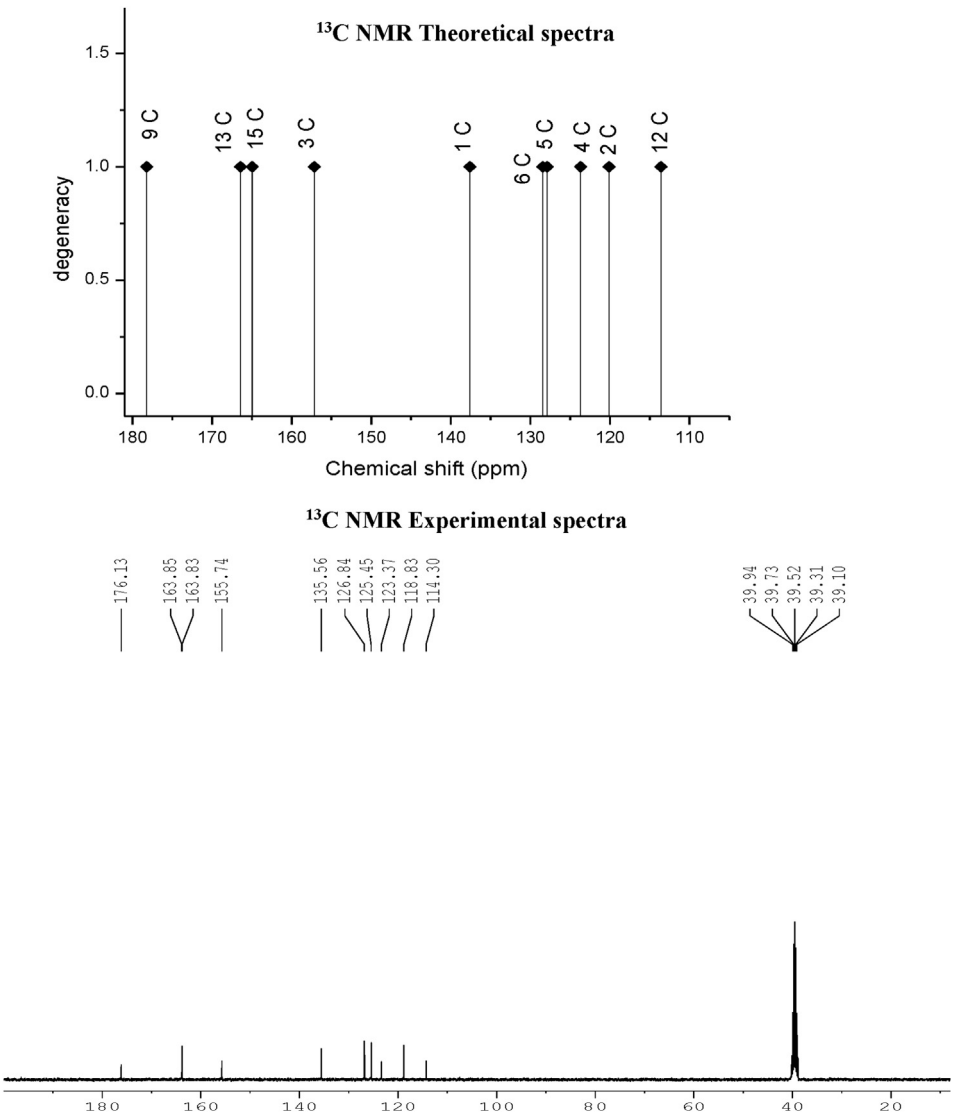

Figure 4. ^{13}C NMR Theoretical and Experimental Spectra of Chromone-3-carboxylic acid.

convex regions indicating the ring atoms of the molecule inside the surfaces. The red triangles on the shape index mapping are referring to the C_2–H_8···π interaction with the contribution of 42.4%. The curvedness is a measure of the shape of the surface area of the molecule. The flat areas of the surface correspond to low values of curvedness, while sharp curvature areas correspond to high values of curvedness indicating the interactions between neighboring molecules. The large flat region which delineated by a blue outline refer to the π···π stacking interactions. The curvedness of the compound reveals that π···π stacking interaction is absent.

4.7. NBO analysis

To study the inter and intra molecular interactions, charge transfer from electron donor to acceptor, the NBO analyses were made. The fock matrix was elucidating in the donor-acceptor interactions in the NBO analysis [20].

The high stabilization energy of the transitions gives a measure of the probabilities of the transitions. In this molecule, the top ten highly probable transitions can be listed as follows in the descending order, based on the stablisation energy: O_{17} to C_{15}–O_{18} (n -σ *, 30.33Kcal/mol), O_{18} to C_{15}–O_{17} (n -π *, 25.15Kcal/mol), O_{19} to C_{12}–O_{13} (n -π *, 20.15Kcal/mol), O_{16} to C_9–C_{12} (n -σ*, 19.58Kcal/mol), O_{19} to C_3–C_4 (n -π *, 18.52Kcal/mol), O_{17} to C_{12}–C_{15} (n -σ*, 17.23Kcal/mol, C_3–C_4 to C_9–O_{16} (π -π*, 17.16Kcal/mol), C_{12}–C_{13} to C_9–O_{16} (π -π*, 15.94Kcal/mol), C_{12}–C_{13} to C_{15}–O_{17} (π -π*, 15.37Kcal/mol) and O_{17} to C_{12}–C_{15} (π -π*, 15.27Kcal/mol). The highest probable transition is O_{17} to C_{15}–O_{18} (n -σ *, 30.33Kcal/mol). Furthermore, most of the above transitions will not appear in UV-Visible spectra due to the forbidden nature of the transitions. Only a very few transitions will be allowed by the selection rules, which can be predicted by HOMO- LUMO analysis; the peaks appeared both in theoretical and experimental spectra are identified with the help of the oscillator strengths of the bands. Table 5 gives the details about the types of bond, acceptors, donors, occupancy levels, energy (E_2), energy difference with polarized energy.

4.8. Electronic properties

4.8.1. Electronic absorption spectra

UV-Visible spectra of C3CA have been analysed with theoretical calculations, major contributions were designated with Swizard program [28] and tabulated in Table 6. The UV- Experimental and theoretical

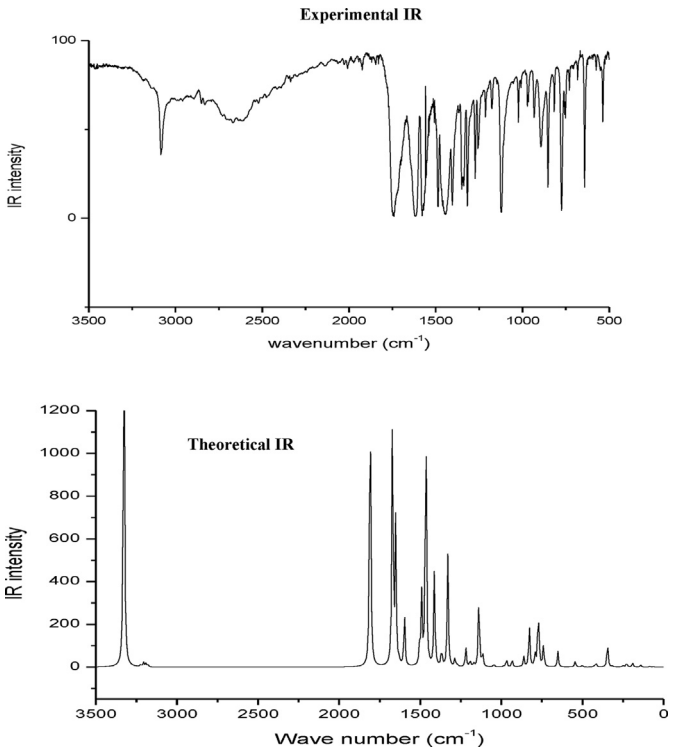

Figure 5. Experimental and theoretical Infrared spectra of chromone-3-carboxylic acid.

spectra are presented in Figure 9. According to the Table.6 the top ten most probable transitions at gas phase have absorption wavelengths 308, 285, 281, 263, 260, 245, 241, 239, 223, 220 nm and their energy gaps are 4.0218, 4.3370, 4.3981, 4.6991, 4.7650, 5.0422, 5.1295, 5.1740, 5.5485, 5.6253 eV respectivelyy, and corresponding oscillator strengths are 0.0001, 0.0000, 0.0627, 0.0000, 0.0019, 0.0447, 0.0001, 0.2923, 0.0435, 0.0810. The oscillator strength 0.0000 shows singlet transition also the gaussian software reflects as 0.0000 when the oscillator strength value is lower than 0.0001. The observation of oscillator strength and absorption co-efficient values indicate that only the third transition will have the appreciable intensity of absorption, which means the peak at 281 nm wavelength will have the maximum intensity, as its HOMO-LUMO contribution is 89%.

Similarly, for DMSO phase in which the experimental spectrum was also recorded, the respective absorption wavelengths are 291, 288, 267, 253, 252, 241, 232, 231, 226, 214 nm with energy gaps 4.25, 4.27, 4.62, 4.88, 4.90, 5.12, 5.32, 5.36, 5.49, 5.77 ev respectively along the oscillator strengths of 0.0001, 0.0786, 0.0068, 0.0000, 0.3693, 0.0000, 0.2091, 0.0001, 0.1555, 0.2034 respectively. In this case, the second transition has the highest HOMO-LUMO contribution of 91%. The theoretical wavelength for this absorption is 288 nm, which appeared at 305 nm in experimental UV spectrum. The deviation from the experimental value may be due to the solvent effect. This transition (H→L) which takes place in both phases is due to n - π * transitions; O_{18} to C_{15}–O_{17} (n -π *, 25.15Kcal/mol) and O_{19} to C_{12}–O_{13} (n -π *, 20.15Kcal/mol). The pictorial representation of DOS of C3CA molecule is plotted in Figure 8 using the GaussSum3 program [29].

4.8.2. Frontier molecular orbital analysis

The diagram of HOMO and LUMO for the title molecule is shown in Figure 10 and the positive negative phases are represented in red and green colour where green indicates the strongest attraction & red indicates the strongest repulsion. From the Figure 10, the HOMO is localized over the C=C bond in the benzene ring but the LUMO is located over the oxygen atoms of the pyrone ring. Hence the HOMO → LUMO electron density transfer occurs from pyrone ring to carboxylic acid group. The transition from the ground state to first excited state occurs from HOMO to LUMO. HOMO has the energy of 5.6844eV while LUMO has 2.735 eV and the energy gap between HOMO to LUMO molecular orbital is 2.9494eV.

4.8.3. Molecular electrostatic potential (MEP)

The MEP map for C3CA molecule is as shown in Figure 11 and it is evident that the strongest affinity for a proton was observed at the carboxylic acid site with the maximum negative region (electrophilic) shown in red color a while the maximum positive region (nucleophilic) referred in blue color around the chromone ring indicating the strongest affinity for electron. Also, the O_{19} atom possess neutral potential while O_{16}, O_{17} and O_{18} are highly repulsive potential. Moreover, H_7, H_8, H_{10} and H_{11} are strongly attractive in nature. The positive and negative potential of the molecule ranges from -6.138e-2 au. to 6.138e-2 au. It is also clear that the blue color are delocalized over the entire chromone ring which offer multiple binding sites through electron acceptance and donation.

4.8.4. Global reactivity descriptors

Table 7 shows the calculated values of the global reactivity descriptors for the title molecule. The calculation of DFT based reactivity descriptors namely, global hardness (η), global softness (S), electronegativity (χ), electrophilicity index (ω) are important to describe the reactivity and site selectivity of various bio-molecules. The electrophilicity is used to predict the biological activities, toxicity and various properties of the molecule. In particular, the energy of the LUMO+1 orbital, electrophilicity and van der Waals surface area are related to biological activities of the molecule.

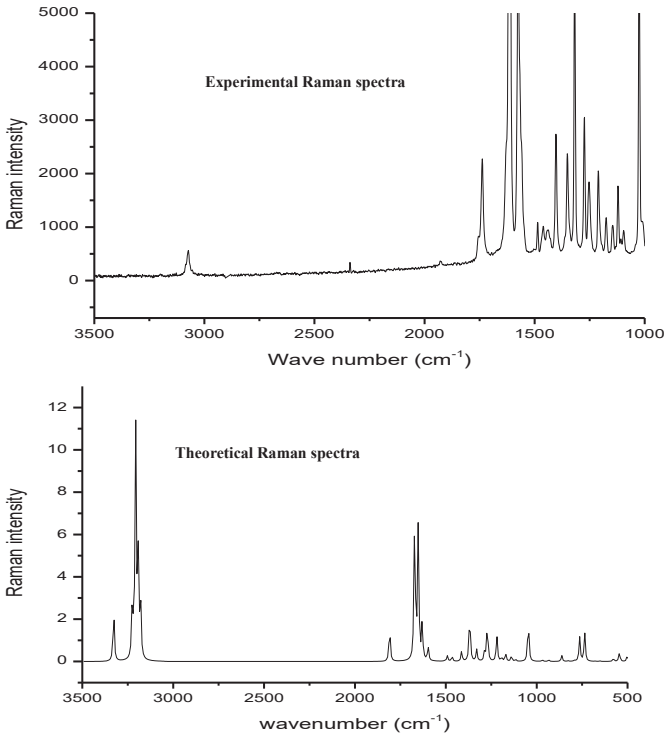

Figure 6. Experimental and Theoretical Raman spectra of chromone-3-carboxylic acid.

Table 4. Experimental and Theoretical (B3LYP 6–311++G (d,p)) vibrational frequencies of Chromone-3-carboxylic acid.

Symmetry species (C_s)	Experimental frequency (cm^{-1})		B3LYP 6-311++G (d,p)	Assignment	PED%
	FT-IR	FT-RAMAN	Scaled (cm^{-1})		
A′	3183		3194	ν OH	ν OH (99)
A′	3089		3095	ν CH	ν CH (99)
A′		3073vw	3078	ν CH	ν CH (99)
A′	3071m		3074	ν CH	ν CH (97)
A′	3062m		3063	ν CH	ν CH (98)
A′	3052 m		3051	ν CH	ν CH (96)
A′	1737s	1734w	1736	ν C=O	ν OC (77)
A′	1615s	1608vs	1604	ν C=O	ν OC (51)
A′		1580w	1584	ν C=C	ν CC (22)
A′	1562s		1563	ν C=C	ν CC (23)
A′		1544w	1533	ν C=C	ν CC (26)
A′		1438w	1443	β OH	ν CC (11) HOC(18) + δ OH (40)+ HCC(14)
A′	1432s		1431	ν C=C	í CC (10)
A′		1402w	1406	ν C–O	δ HOC(74)
A′		1360w	1355	ν C–O	ν OC (10)
A′		1320w	1313	ν C–O	ν CC (17) + δ HCO (10) OC(74)
A′	1263m	1260w	1276	ν C–C	δ HCO (38)
A′	1251m	1248w	1234	ν C–C	δ HCC(17) + δ HCO (10)
A′		1225w	1220	ν C–C	ν OC (20)+ ν CC (10)
A′	1183w	1177w	1170	ν C–C	ν OC (12) HCC(34)
A′		1130w	1144	ν C–C	ν CH (25) + ν CC (11) + δ CCC(10)
A′	1110s		1123	ν C–C	ν OC (11) + δ HCC (21)
A′		1095vw	1092	δ CH	ν OC (23)
A′	1089w		1070	δ CH	δ CCH (50) + δ CCC (13)
A′	1017w	1012w	1004	δ CH	ν CC (45)+ â HCC (40)
A′		953w	969	δ CH	δ CCCH (11)
A′	940m		946	δ CH	δ HCCH (43) + δ CCCH (37)
A′		926vw	929	δ C=O	δ HCOC(79)
A′	898m		895	δ C=O	ν CC (13) + δ CCO (23)
A′	847s	849w	849	δ OH	δ CCCH (45)
A″	813s	811w	826	δ C–O	δ CCC (40) + δ COC (14)
A″		799w	793	δ C–C	δ HOCC (83)
A″		794w	760	δ CH	δ CCCH (17)
A″	751s	740w	741	δ CH	δ CCCH (12)
A″		728w	732	δ CH	δ OCH (14)
A″	697w		712	δ CH	δ CCCH(15)
A″		689w	705	δ CH	δ OCH (38)
A″	643vw	642vw	649	δ C=O	δ CCCC (10)
A″	620s		624	δ C=O	δ CCO (19) + δ CCC (20)
A′	548m		553	δ C–O	δ OCO (21)
A′		538w	527	δ C–C	δ OCCC (40)
A′	525w		522	δ COH	δ CCC (34) + δ OC (13) + δ CCC (31)
A′		480w	480	δ CCC	δ CCC(38) + δ CCO (14)
A′		445w	443	δ CCC	δ CCC(14) + δ CCC (11)
A′	426m	408w	411	δ CCC	δ CC(15)+ δ CCO (43)
A′	386m		399	δ CCC	δ CCCC(27)+ δ CCOC (17)
A′	332s		331	δ CCO	δ CCO (13)
A″		306m	304	δ COC	δ CC(19) + δ CCC (11)
A″		230w	238	δ CCC	δ CCCC(23)
A″		220w	217	δ CCO	δ CCOC (21)
A″		184w	182	δ CCC	δ CCC (10)
A″		137w	134	δ CCO	δ CCCC(49)
A″		78s	81	δ CCO	δ CCCO(72)
A″		66s	56	δ COC	δ CCCO (24)

ν–stretching; β–in–plane bending; δ–deformation; ρ–rocking; γ–out of plane bending; ω–wagging and τ–torsion. IR and Raman intensities are normalized to 100.

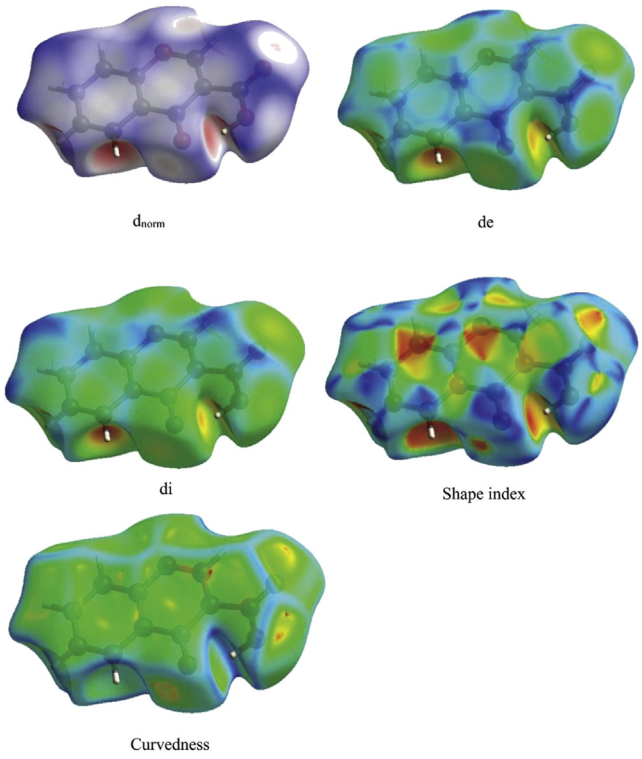

Figure 7. Hirshfeld surface for d-norms, de, di, shape index and curvedness of chromone-3-carboxylic acid.

Electrophilicity index (ω) is considered as a measure of electrophilic power of a molecular system towards a nucleophile. If higher the electrophilicity index, higher will be the reactivity as an electrophile while if it is lower, more reactivity as nucleophile. In the present study, we have calculated the electrophilicity index as 6.32 ev which is greater demonstrates that the molecule has higher reactivity as an electrophile.

According to MHP, at constant external potential the stability of a molecule increases with hardness and with the increase in stability the reactivity decreases. The value of chemical hardness calculated in this study is -1.4747eV (gas phase). Here we have calculated the chemical hardness as -1.4747eV (gas phase) while the global softness is 5.8988 ev shows that the molecule has soft in nature and the small HOMO-LUMO energy gap (2.9494 ev) implies that the molecule is more reactive.

4.9. Docking study

In docking, the host is the receptor (protein) and the binder is the title compound (ligand). Docking calculations were performed on Auto Dock software [30] and visualized through Discovery Studio Visualizer software 4.0 [30]. The optimized structure of C3CA was docked with the protein 4UAR of Bacillus subtilis. The 3D crystal structure of protein -ligand interaction was obtained from PDB (PDB ID: 4UAR). The active site of the protein ligand interaction is shown Figure 12 with grid size of 90 Å x 90 Å x 90 Å.

The docking positions with lowest docking energy (binding affinity) is studied and the bond lengths at these positions were calculated by RMSD method and the values are presented in Table 8. RMSD values above to 2 Å are considered reliable for hydrogen bond formation in docking protocol. Different sets of hydrogen bonding interactions with polar side chain residues of AAR 162, and non-polar residue of LEU159 are observed at distances around 2Å ie., 2.4 Å and 2.1 Å respectively. The ligand binding sites for various modes of interactions with the protein is shown in Figure 12.

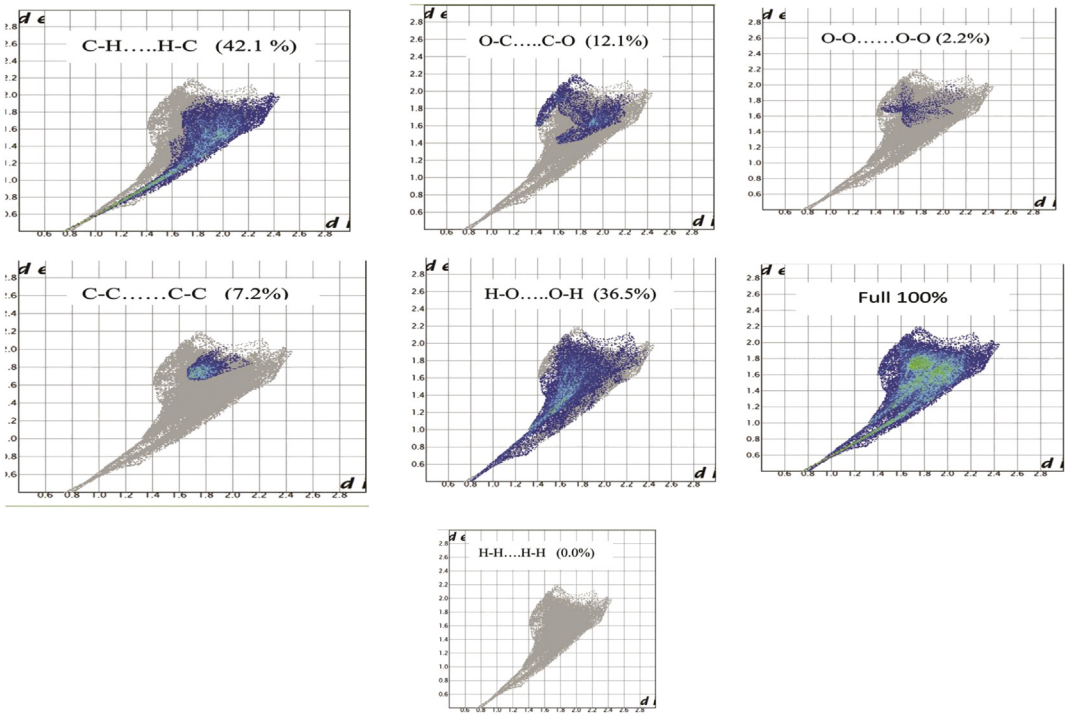

Figure 8. Finger print of total Hirshfeld, O–C···C–O, H–O….O–H, C–C….C–C, C–H….H–C, H–H….H–H, O–O….O–O.

Table 5. Natural Bonding Orbital energy profile of Chromone-3-Carboxylic Acid.

Donor	Type of bond	Occupancy	Acceptor	Type of bond	Occupancy	Energy E (2) kcal/mol	Energy difference E(j)-E(i) a.u.	Polarized energy F (i,j) a.u.
C_1–C_2	σ	1.98152	C_3–O_{19}	σ*	0.03344	2.89	0.98	0.048
C_1–C_2	π	1.82167	C_3–C_4	π*	0.2694	11.25	0.3	0.053
C_1–C_2	π	1.82167	C_5–C_6	π*	0.14554	9.42	0.32	0.049
C_1–C_6	σ	1.97879	C_2–H_8	σ*	0.01116	3.15	1.06	0.052
C_1–C_6	σ	1.97879	C_5–H_{10}	σ*	0.01078	3.03	1.08	0.051
C_1–H_7	σ	1.97941	C_2–C_3	σ*	0.02878	5.4	0.91	0.063
C_2–C_3	σ	1.9742	C_1–H_7	σ*	0.01022	2.57	1.09	0.047
C_2–C_3	σ	1.9742	C_3–C_4	σ*	0.01116	2.74	1.25	0.052
C_2–C_3	σ	1.9742	C_4–C_9	σ*	0.06074	3.85	1.04	0.057
C_2–H_8	σ	1.97925	C_1–C_6	σ*	0.02117	5.05	0.93	0.061
C_3–C_4	π	1.75875	C_1–C_2	π*	0.16418	9.01	0.32	0.049
C_3–C_4	π	1.75875	C_5–C_6	π*	0.14554	9.42	0.33	0.051
C_3–C_4	π	1.75875	C_9–O_{16}	π*	0.20158	17.16	0.3	0.064
C_4–C_5	σ	1.96596	C_3–C_4	σ*	0.01116	3.04	1.23	0.055
C_4–C_5	σ	1.96596	C_3–O_{19}	σ*	0.03344	5.84	0.85	0.063
C_4–C_5	σ	1.96596	C_6–H_{11}	σ*	0.01109	2.88	1.08	0.05
C_4–C_9	σ	1.97599	C_2–C_3	σ*	0.02878	3.92	1.02	0.057
C_5–C_6	π	1.81447	C_1–C_2	π*	0.16418	11.61	0.3	0.053
C_5–C_6	π	1.81447	C_3–C_4	π*	0.2694	11.15	0.29	0.052
C_5–H_{10}	σ	1.97834	C_1–C_6	σ*	0.02117	5.24	0.92	0.062
C_5–H_{10}	σ	1.97834	C_3–C_4	σ*	0.01116	2.54	1.14	0.048
C_6–H_{11}	σ	1.98034	C_4–C_5	σ*	0.02396	5.23	0.92	0.062
C_9–C_{12}	σ	1.97383	C_{13}–H_{14}	σ*	0.01668	2.75	1.04	0.048
C_9–O_{16}	π	1.96403	C_{12}–C_{13}	π*	0.1534	5.75	0.35	0.041
C_{12}–C_{13}	π	1.84517	C_9–O_{16}	π*	0.20158	15.94	0.32	0.065
C_{12}–C_{13}	π	1.84517	C_{12}–C_{13}	π*	0.1534	2.55	0.31	0.025
C_{12}–C_{13}	π	1.84517	C_{15}–O_{17}	π*	0.19384	15.37	0.31	0.062
C_{12}–C_{15}	σ	1.97604	C_{13}–O_{19}	σ*	0.02683	4.63	0.89	0.057
C_{13}–H_{14}	σ	1.98137	C_9–C_{12}	σ*	0.06758	4.82	0.99	0.062
C_{15}–O_{17}	π	1.97381	C_{12}–C_{13}	π*	0.1534	5.56	0.36	0.041
O_{18}–H_{20}	σ	1.98175	C_{15}–O_{17}	σ*	0.01624	3.04	1.28	0.056
O_{16}	n	1.88826	C_4–C_9	σ*	0.06074	17.23	0.65	0.095
O_{16}	n	1.88826	C_9–C_{12}	σ*	0.06758	19.58	0.64	0.101
O_{17}	n	1.84395	C_{12}–C_{15}	σ*	0.06674	15.27	0.6	0.088
O_{17}	n	1.84395	C_{15}–O_{18}	σ*	0.10554	30.33	0.49	0.111
O_{18}	n	1.9753	C_{12}–C_{15}	σ*	0.06674	4.89	0.99	0.063
O_{18}	n	1.87016	C_{15}–O_{17}	π*	0.19384	25.15	0.34	0.084
O_{19}	n	1.97109	C_3–C_4	σ*	0.01116	4.33	1.21	0.065
O_{19}	n	1.97109	C_{12}–C_{13}	σ*	0.01679	3.61	1.18	0.058
O_{19}	n	1.78958	C_3–C_4	π*	0.2694	18.52	0.39	0.077
O_{19}	n	1.78958	C_{12}–C_{13}	π*	0.1534	20.15	0.36	0.078

Table 6. Theoretical electronic absorption spectra of chromone-3-carboxylic acid (absorption wavelength λ (nm), excitation energies E (ev) and oscillator strengths (f) using TD-DFT/B3LYP/6–311++G (d,p) method.

λ (nm) Theoretical Gas	Experimental	E (eV)	(f)	Major contribution
308		4.0218	0.0001	H-1→LUMO (60%)
285		4.3370	0.0000	H-2→LUMO (55%)
281		4.3981	0.0627	HOMO→LUMO (89%)
263		4.6991	0.0000	H-1→L+1 (80%)
260		4.7650	0.0019	HOMO→L+1 (50%)
245		5.0422	0.0447	H-4→LUMO (60%)
241		5.1295	0.0001	H-2→L+1 (97%)
239		5.1740	0.2923	HOMO→L+1 (41%)
223		5.5485	0.0435	H-5→LUMO (74%)
220		5.6253	0.0810	H-3→L+1 (30%)

Table 6 (*continued*)

λ (nm) Theoretical Gas	Experimental	E (eV)	(f)	Major contribution
DMSO				
291		4.2510	0.0001	H-2→LUMO (91%)
288	305	4.2775	0.0786	HOMO→LUMO (91%)
267		4.6258	0.0068	H-1→LUMO (46%)
253		4.8826	0.0000	H-4→LUMO (45%)
252		4.9055	0.3693	H-1→LUMO (44%)
241		5.1287	0.0000	H-4→LUMO (39%)
232		5.3224	0.2091	H-3→LUMO (76%)
231		5.3658	0.0001	H-4→L+1 (80%)
226		5.4972	0.1555	H-3→L+1 (13%)
214		5.7793	0.2034	H-3→L+1 (63%)

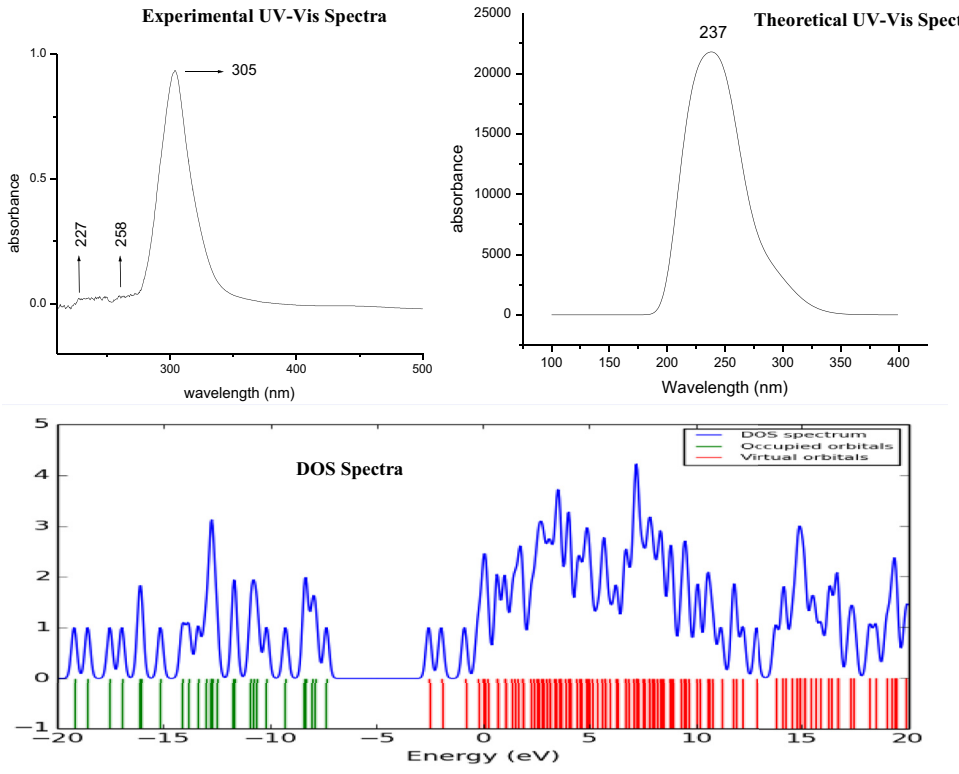

Figure 9. Experimental, Theoretical UV-Vis Spectra & DOS spectra of chromone-3-carboxylic acid.

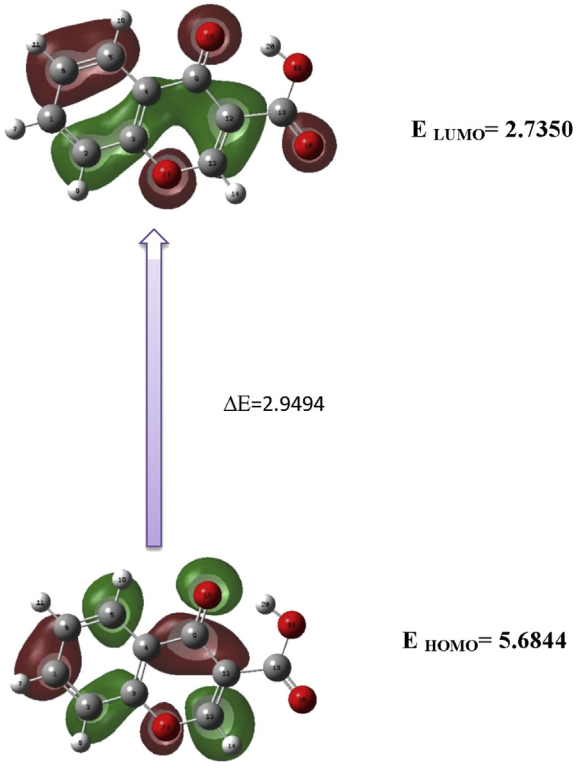

Figure 10. Frontier molecular orbitals of chromone-3-caboxylic acid.

Table 7. Homo, Lumo, Kubo gap, global electro negativity, global hardness and softness, global electrophilicity index of Chromone-3-Carboxylic acid.

Parameters	Gas
E_{HOMO} (ev)	5.6844
E_{LUMO} (ev)	2.7350
$\Delta E_{HOMO\text{-}LUMO\ gap}$ (ev)	2.9494
Elecronegativity (÷) (ev)	-4.2090
Global hardness (ç) (ev)	-1.4747
Global softness (S) (ev)	5.8988
Electrophilicity index (ω) (ev)	6.3200
Dipole Moment (μ) (debye)	7.7040

Table 8. Interaction between Anti-bacterial Sugar-phosphatase inhibitor with target protein 4UAR.

Protein (PDB ID)	No.of hydrogen bond	Bonded Residues	Bond Distance Å
4UAR	3	AAR 162	2.4
		AAR 162	2.4
		LEU159	2.1

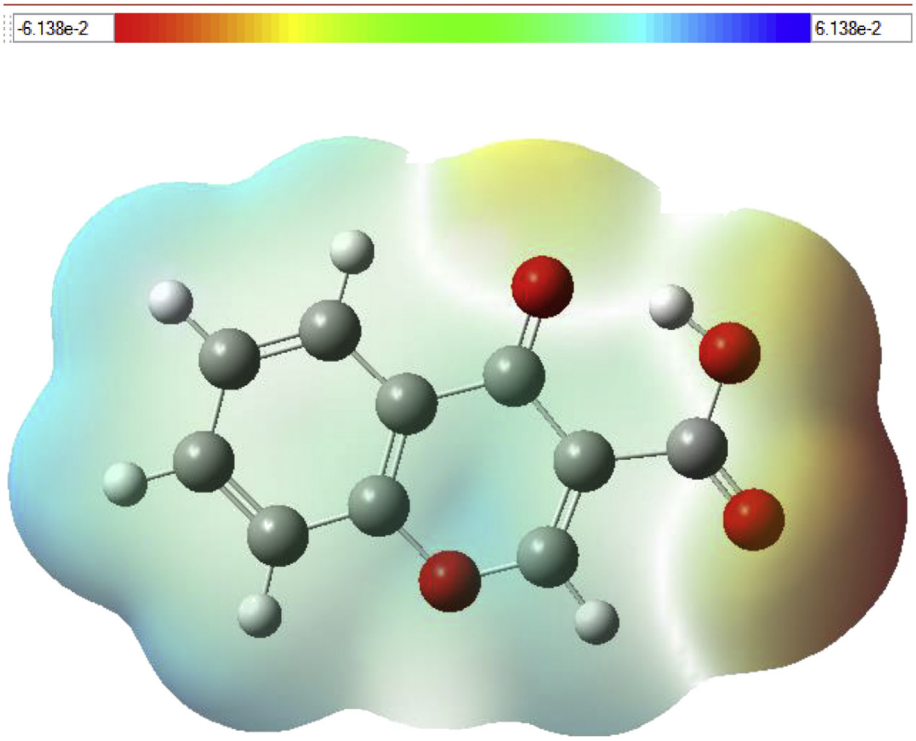

Figure 11. Molecular electrostatic potential map of chromone-3-carboxylic acid.

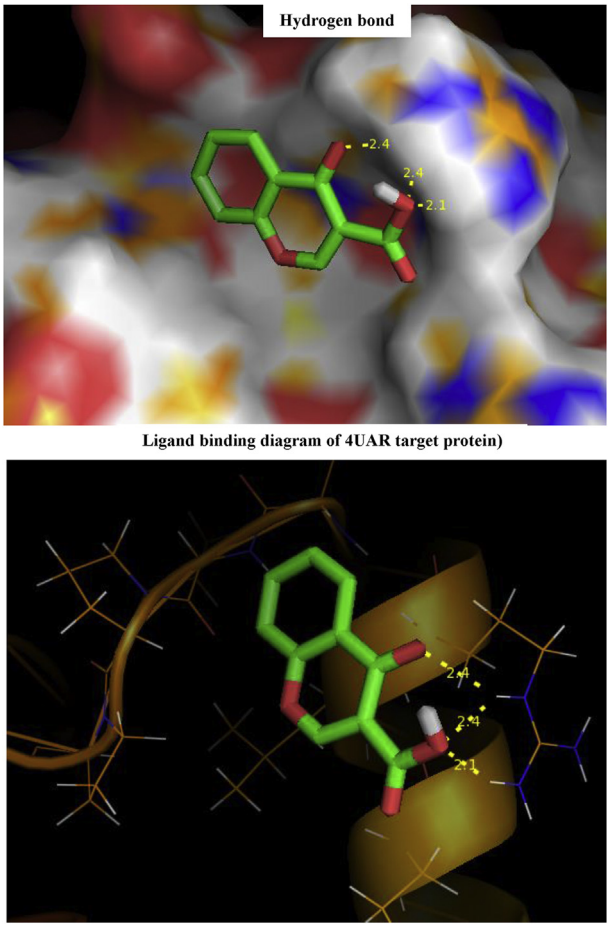

Figure 12. Hydrogen bond, ligand binding diagram of 4UAR target protein with ligand.

5. Conclusion

The presence of carboxylic group decreases the electron density in the chromone ring system which consists of benzene and pyrone rings. The conformational analysis was performed by Potential Energy Surface Scan (PES) to predict the stable conformer. The minimum energy of the compound was found to be -0.190 hartree at 360^{o} respectively. From the MPA it is confirmed that the charge of carbon atoms in the benzene ring were redistributed due to the substitutional groups. The charges predicted by MPA were found supported by the chemical shift analysis from the NMR study. From NBO analysis, the most probable transitions in the molecule are identified. The vibrational wavenumbers computed theoretically were found agreeing well with the experimental values. UV-Visbile analysis of the compound indicates that among the ten probable electronic transitions, only the second and third transitions in the list will have the appreciable intensity of absorption. From HOMO & LUMO analysis, global reactivity descriptors, it is confirmed that the molecule is considered as soft (as the energy gap is less), has higher reactivity as an electrophilic (higher electrophilicity index), more reactive (hardness is less). The MEP analysis implied that the skeleton of the benzene ring and edges of the molecule shows more zero potential regions. The molecule is also analysed, and the molecular docking was made with the protein of 4UAR of Bacillus subtilis. The antioxidant and bioactive nature of this molecule which neutralize the active nature of oxygen and reducing free radical process makes this molecule as a active candidate for anti-inflammatory, antifungal, antimicrobial, antiviral, antitumour and anticancer drugs.

Declarations

Author contribution statement

K. Jayasheela: Performed the experiments.

S. Periandy: Contributed reagents, materials, analysis tools or data.

P.B. Nagabalasubramanian: Conceived and designed the experiments; Performed the experiments; Analyzed and interpreted the data; Contributed reagents, materials, analysis tools or data; Wrote the paper.

Funding statement

This research did not receive any specific grant from funding agencies in the public, commercial, or not-for-profit sectors.

Competing interest statement

The authors declare no conflict of interest.

Additional information

No additional information is available for this paper.

Acknowledgements

We remain grateful to Kanchi Mamunivar Govt. Institute for Post Graduate Studies and Research, Lawspet, Puducherry and the Department of Physics, St. Joseph's College of Arts and Science (Autonomous), Cuddalore for providing the Quantum Computational Research Lab for this study.

References

[1] N. Phosrithong, W. Samee, P. Nunthanavanit, J. Ungwitayatorn, *In vitro* antioxidant activity study of novel chromone derivatives, Chem. Biol. Drug Des. 79 (2012) 981–989.
[2] yu Mikhail, Vyacheslav Kornev, Synthesis and chemical properties of chromone-3-carboxylic acid, Chem. Heterocycl. Compd. 52 (2016) 71–83.
[3] J.G. Teixeira, C.B. Dias, D.M. Teixeira, Electrochemical characterization and quantification of the strong antioxidant and antitumor agent pomiferin, Electroanalysis 21 (2009) 2345.
[4] I. Sabel, P.G. Fernandes, **Electrochemical oxidation mechanisms of the antioxidants daidzein and 7-hydroxy-4-chromone**, Electroanalysis 24 (3) (2012) 618–626.
[5] J. Liang, Y.X. Tian, L.M. Fu, T.H. Wang, **Daidzein as an antioxidant of lipid: Effects of the microenvironment in relation to chemical structure**, Agr. Food Chem. 56 (2008) 10376.
[6] A. Aliabadi, F. Shamsa, S. Ostad, Synthesis and biological evaluation of 2-phenylthiazole-4-carboxamide derivatives as anticancer agents, Eur. J. Med. Chem. 45 (2010) 5384.
[7] S. Sebastian, Molecular structure, Normal Coordinate Analysis, harmonic vibrational frequencies, Natural Bond Orbital, TD-DFT calculations and biological activity analysis of antioxidant drug 7-hydroxycoumarin, Spectrochim. Acta Part A Mol. Biomol. Spectrosc. 101 (2013) 370–381.
[8] M.M. Dias, Dietary chromones as antioxidant agents—the structural variable, Food Func. 2 (2011) 595.
[9] A. Magdy Ibrahim, Ring transformation of chromone-3-carboxylic acid under nucleophilic conditions, J. Arkivoc 17 (2008) 192–204.
[10] M. Agostinha, R. Matos, S. Sousa, F. Morais, Thermochemistry of chromone- and coumarin-3-carboxylic acid, J. Therm. Anal. Calorim. 100 (2010) 519–526.
[11] R. Sahan, Modulating the reactivity of chromone and its derivatives through encapsulation in a self-assembled phenylethynylene *bis*-urea host, Salp. J. Photochem. Photobiol. A: Chem. 315 (2016) 14–24.
[12] Shahriarkhadem, Chromone and flavonoid alkaloids: Occurrence and bioactivity, J. Molec. 17 (2012) 191–206.
[13] A. Magdy, Synthesis and chemical reactivity of 2-methylchromones, Ibrahim J. Arkivoc (2010) 98–135.
[14] K. Jayasheela, S. Periandy, S. Xavier, K. Niveditha, Docking and spectral investigations (FT-IR, FT-Raman, NMR, UV-Vis) on 7-hydroxyl-4-chromone using quantum computational (DFT) analysis, Int. J. Renew. Energy Technol. (2017).
[15] M.J. Frisch, et al., GAUSSIAN 09, Revision A.1, Gaussian, Inc., Wallingford, CT, 2009.
[16] M.H. Jamroz, Vibrational Energy Distribution Analysis VEDA 4, Warsaw, 2004–2010.
[17] A. Frisch, A.B. Nielson, A.J. Holder, GAUSSVIEW User Manual, Gaussian Inc., Pittsburgh, PA, 2000.
[18] Y. Ishikawa, et al., Topic crystal structure of 3-(hy-dr-oxy-meth-yl)chromone, J. Acta Cryst. E 496 (2015) 580–591.
[19] P.B. Nagabalasubramanian, M. Karbacak, S. Periandy, Molecular structure, polarizability, characterization hyperpolarizability analysis and spectroscopic of 1-(chloromethyl)-2-methylnaphthalene (FT-IR with experimental and FT-Raman) techniques and quantum chemical calculations, Spectrochim. Acta Part A 85 (2012) 43–52.
[20] G. Mariappan, N. Sundaraganesan, FT-IR, FT-Raman, NMR spectra, density functional computations of the vibrational assignments (for monomer and dimer) and molecular geometry of anticancer drug 7-amino-2-methylchromone, J. Mol. Struct. 1063 (2014) 192–202.
[21] P.B. Nagabalasubramanian, S. Periandy, Mehmet Karabacak, M. Govindarajan, Molecular structure, vibrational, electronic and thermal properties of 4-vinylcyclohexene by quantum chemical calculations, Spectrochim. Acta Mol. Biomol. Spectrosc. 145 (2015) 340–352.
[22] R. Ditchfield, Molecular orbital theory of magnetic shielding and magnetic susceptibility, J. Chem. Phys. 56 (1972) 5688–5691.
[23] K. Wolinski, J.F. Hinton, P. Pulay, Efficient implementation of the gauge-independent atomic orbital method for NMR chemical shift calculations, J. Am. Chem. Soc. 112 (1990) 8251–8260.
[24] H.O. Kalinowski, S. Berger, S. Braun, Carbon-13 NMR Spectroscopy, John Wiley &Sons, Chicheser, 1988.
[25] L.G. Wade (Ed.), Journal of Advanced Organic Chemistry, fourth ed., Wiley, New York, 1992, p. 723.
[26] N.P.G. Roeges, A Gide to the Completer Interpretation of Infrared Specra of Organic Structures, Wiley, New York, 1994.
[27] M.M. Garrett, S.G. David, s.H. Rober, H. Ruth, E.H. William, K.B. Richard, J.O. Arthur, Automated docking using a Lamarckian genetic algorithm and an empirical binding free energy function, J. Comput. Chem. 19 (1998) 1639–1662.
[28] S.I. Gorelsky, SWizard Program Revision 4.5, University of Ottawa, Ottawa, Canada, 2010. http://www.sg.chem.net.
[29] N.M. O'Boyle, A.L. Tenderholt, K.M. Langner, cclib: A library for package-independent computational chemistry algorithms, J. Comp. Chem. 29 (2008) 839–845.
[30] K. Jayasheela, S. Periandy, Probing vibrational activities, electronic properties, molecular docking and Hirshfeld surfaces analysis of 4-chlorophenyl ({[(1*E*)-3-(1*H*-imidazol-1-yl)-1-phenylpropylidene]amino}oxy)methanone: A promising anti-*Candida* agent, J. Mol. Struct. 1159 (2018) 83–95.